Simulating the out-of-equilibrium dynamics of local observables by trading entanglement for mixture

J. Surace,[1] M. Piani,[1] and L. Tagliacozzo[1,2]

[1]*Department of Physics and SUPA, University of Strathclyde, Glasgow G4 0NG, United Kingdom*

[2]*Departament de Física Quàntica i Astrofísica and Institut de Ciències del Cosmos (ICCUB), Universitat de Barcelona, Martí i Franquès 1, 08028 Barcelona, Catalonia, Spain*

(Received 10 October 2018; published 7 June 2019)

The fact that the computational cost of simulating a many-body quantum system on a computer increases with the amount of entanglement has been considered as the major bottleneck for simulating its out-of-equilibrium dynamics. Some aspects of the dynamics are, nevertheless, robust under appropriately devised approximations. Here we present a possible algorithm that allows to systematically approximate the equilibration value of local operators after a quantum quench. At the core of our proposal, there is the idea to transform entanglement between distant parts of the system into mixture, and at the same time preserving the local reduced density matrices of the system. We benchmark the resulting algorithm by studying quenches of quadratic fermionic Hamiltonians.

DOI: 10.1103/PhysRevB.99.235115

I. INTRODUCTION

Simulating the time evolution of many-body quantum systems by classical means is hard. In fact, simulating an N constituents system requires storage and computation time that scale exponentially with N. As an example, consider the exponentially large space needed in order to store the 2^N complex coefficients describing the state of a $1/2$ spin chain of length N.

In some cases, the specific structure of the problem allows to devise efficient classical algorithms for simulating many-body systems. For example, in the context of statistical mechanics, a many-body system can have exponentially many configurations. However, in most cases, using Monte Carlo algorithms, we can sample only a polynomially large set of those configurations, thus simulating the system efficiently [1].

In the context of many-body quantum systems at equilibrium, the locality of correlations [2–4] can be exploited in order to design efficient algorithms based on tensor networks. The exponential decay of correlations in the relevant states at equilibrium, i.e., the ground and thermal states of gapped local Hamiltonians implies that these states only have a limited amount of entanglement [2,3]. Their entanglement grows only proportionally to the boundary of a region rather than its volume, a phenomenon formalized in the area law of entanglement [4–7]. States whose entropy fulfils the area law, generally, can be efficiently described by tensor networks and manipulated by appropriate algorithms. The most notable examples are DMRG [8,9] and its higher-dimensional generalisations (see, e.g., Refs. [6,10]). DMRG, as of today, provides the most accurate results for strongly correlated one-dimensional quantum systems.

The locality of correlations is lost in the context of many-body quantum systems out-of-equilibrium. In particular it is lost in the dynamics induced by a quench of the Hamiltonian. In this scenario, initially localized correlations can be radiated to arbitrarily large distances [11,12] leading to a fast growth of entanglement with time [13–18]. As a consequence, traditional tensor network approaches fail to encode the states generated during the out-of-equilibrium dynamics at relatively short times [19].

Here we focus on encoding locally the states generated during the out-of-equilibrium dynamic, rather than trying to encode the full states. We design an algorithm aiming at reproducing locally the out-of-equilibrium dynamics for arbitrarily long times.

The algorithm is designed with tensor networks in mind, but here we start benchmarking it in the context of noninteracting systems where we can also compute the full out-of-equilibrium dynamics.

The performances of tensor-network algorithms mostly depend on the amount of entanglement contained in the states they try to describe. The strength of the interactions in a specific Hamiltonian does not necessarily affect the amount of entanglement between the constituents in its ground state. For example, ground states of free systems can be robustly entangled (think, e.g., about a Fermi see in momentum space) while strongly interacting Hamiltonians can have product ground states (think, e.g., about the ground state of a Mott insulator).

The use of noninteracting systems is thus often seen as a first benchmark for tensor network algorithms (see, e.g.. Ref. [20]). Recently several authors have realized that it is also possible to directly implement tensor network algorithms at the level of the correlation matrices (see, e.g., Refs. [21–25]). This discovery allows to prototype new tensor-network ideas without having to fully implement them. It also allows to decouple the effects caused by the physical approximations contained in the algorithms from those of the spurious approximations that could appear in specific tensor-networks implementations.

For these reasons, here we benchmark a new tensor network algorithm at the level of correlation matrices in the case of free-fermions. In particular, we approximate the out-of-equilibrium dynamics of a free fermionic system by only using its short-range correlations.

This is only possible by trading entanglement with mixture during the out-of-equilibrium evolution (similarly to what happens in the algorithm proposed in Refs. [26,27]). As a result, we can approximate the robustly entangled pure states generated during the evolution with slightly entangled mixed states.

Crucially those mixed states are locally indistinguishable from the pure state they approximate. In this way, we aim at performing the full out-of-equilibrium dynamics in a subspace of slightly entangled states that we can encode with tensor networks.

We show that despite, the rough approximations involved in such an algorithm, we are still able to accurately predict the correct equilibration value of local observables and their approach to equilibrium. This fact relies on the robustness of the equilibration process in spite of ignoring the long-distance correlations generated during the out-of-equilibrium evolution.

II. ROBUST ASPECTS OF QUANTUM QUENCHES

In the following, we focus on the out-of-equilibrium dynamics after a quantum quench [28]. Initially the system is at equilibrium, say in the ground state $|\psi\rangle$ of some local Hamiltonian H. The Hamiltonian is abruptly changed from H to $\tilde{H}$, quenching the system out-of-equilibrium. The corresponding evolution is described by

$$|\psi(t)\rangle = e^{-it\tilde{H}}|\psi\rangle. \tag{1}$$

Cardy and Calabrese [11] showed that in this setting the entanglement entropy between two different partitions of $|\psi(t)\rangle$ grows linearly in time, a footprint of the radiation of the correlation as pseudoparticles [11,29–32]. This leads the corresponding states to become too entangled and hard to represent with standard tensor network algorithms after relatively short times [19,33].[1]

The short-time dynamics is highly nonuniversal and very sensitive to the specific details of the quench.[2] Here we try to address robust features of the out-of-equilibrium dynamics after a quench, that is, features that are not too sensitive to the specific details of the quench. One of such features is the equilibration of local observables occurring at long times after the quench.

In most cases, the values of the relaxed local observables are indistinguishable from those computed on the *diagonal ensemble* (DE) defined as

$$\rho_{\mathrm{DE}(\tilde{H})} := \sum_n |E_n\rangle\langle E_n|\rho|E_n\rangle\langle E_n|, \tag{2}$$

where $\{|E_n\rangle\}_n$ are the eigenvectors of the Hamiltonian $\tilde{H}$ driving the dynamics and ρ encodes the state of the system before the quench. That is, if an observable A equilibrates, at late times after the quench $\langle A(t)\rangle \simeq \mathrm{Tr}[A\rho_{\mathrm{DE}(\tilde{H})}]$. The direct construction of the DE is exponentially hard.

In the generic cases, the DE is locally approximated by a Gibbs Ensemble (GE) as a consequence of the *eigenstate thermalisation hypothesis* (ETH) [34–39]. The temperature of the Gibbs ensemble only depends on the energy of the initial state unveiling a high degree of robustness in the process of thermalisation.

For those systems described by a local Hamiltonian, the energy is conserved if we conserve short-range correlations. As a result, by designing an approximate dynamics conserving short-range correlations, the robustness of the thermalisation process forces the convergence to the correct state, in spite of discarding the long-range correlations.

The free-fermionic systems we use here as a benchmark do not satisfy the ETH, since their relaxed state depends on the initial occupation of all the free modes. These occupations are conserved during the evolution. As a result, the equilibration of these systems is locally described by *generalized Gibbs ensemble* (GGE) rather than by a GE. The GGE can be defined as the state that maximizes the entropy at fixed value of all the conserved quantities [30,31,36,40–47].

The equilibrium state after a quench in free-fermionic systems thus depends on infinitely many parameters. This fact seems to spoil the robustness of the equilibration process. Luckily a weaker notion of robustness can be recovered. The occupation of the free modes can be re-expressed as the conservation of charges whose densities are defined on bounded regions of the lattice. We can thus sort the conserved charges by the dimension of the support of their density. Charges whose densities have support on smaller blocks are more local than those with support on larger blocks.

As shown in Refs. [44,48], the DE is also locally approximated by a truncated version of the GDE. The latter only depends on a finite number of parameters associated with conserved charges built out of density with support smaller than a fixed finite number of sites. The accuracy of the approximation increases by including in the truncated GGE charges with larger and larger supports (see, however, Refs. [49–52] for cases in which this approximation fails).

Our benchmarks with free fermions, thus rely on this weaker notion of robustness. Any algorithm correctly describing short-range correlations is forced by this weaker robustness to convergence to a truncated version of the GGE. We both design and characterize such an algorithm in the following sections.

III. THE ALGORITHM

The algorithm we introduce here is designed to work with tensor-network states. It is inspired by the original time-evolving block decimation algorithm (TEBD) [53] and the time dependent density matrix renormalization group

[1] Here we consider only systems whose excitations are extended and can be described using pseudoparticles. A treatment of different systems such as those described in Ref. [83] will be performed separately.

[2] For a detailed analysis of the universal aspects encoded in the light cone spreading of the correlations after a quench, we refer the reader to Ref. [84].

(t-DMRG) [54]. It exploits both our ability to encode slightly correlated states as tensor networks and to perform, almost exactly, their short-time dynamics.

Differently from all of these algorithms, it ensures that the approximated state (i) has the short-range correlations of the state we want to approximate, (ii) can be encoded with the available resources, and (iii) is a mixed state.

By using (i) we exploit the idea of robustness discussed in the previous section; with (ii) we ensure that the algorithm is practically useful, also at long times. The choice of (iii) is dictated by the observation that both the GE and GGE are mixed states.

For completeness, we start by reviewing standard tensor networks techniques for performing the out-of-equilibrium evolution of 1D systems. The main idea was put-forward by G. Vidal in the paper that introduced the TEBD [53] and was later refined in several key contributions (see, e.g., the recent review on the topic [55]).

Given an initial state $|\psi(0)\rangle$ we want to evolve it for a time t. In formula $|\psi(t)\rangle = \exp(-iHt)\,|\psi(0)\rangle$. Even assuming we know how to encode the initial state (say, e.g., it is a product state in the local basis), we still need to apply to it $U(t) = \exp(-iHt)$, that is an operator that grows exponentially with the size of the system.

The general strategy can be illustrated by restricting to local Hamiltonians (see however [56] for how to extend it to nonlocal ones), $H = \sum_{\langle i,j\rangle} h_{i,j}$, with $h_{i,j}$ the Hamiltonian density acting on constituents i, j that are nearest neighbours on the lattice.

We subdivide the evolution in M small steps $\exp(-iHt) = \exp(\frac{-iHt}{M})^M = \exp(-iH\delta t)^M$ in such a way that $\delta t = t/M$ becomes arbitrarily small. We now have to solve M short-time evolutions from $t_i \to t_i + \delta t$, where $t_i = (i-1)\delta_t$ and $i = 1, \ldots, M$. Each evolution acts on the state that is produced by the previous step.

In order to proceed we now assume that $|\psi(0)\rangle$ is a matrix product state (MPS), that is a state of the form $|\psi(0)\rangle = \sum_{i_1\cdots i_N} c^{i_1\cdots i_N}\,|i_1, \cdots i_N\rangle$ with $c^{i_1\cdots i_N} = \mathrm{tr}(A^{i_1}\cdot A^{i_2}\ldots A^{i_{N-1}}\cdot A^{i_N})$, where each of the A^i is a $D\times D$ matrix.

The A are thus tensors with three indices, that are typically represented by geometric shapes with three attached lines, one for each index (see panel a of Fig. 1). When the indexes are contracted (such as in the matrix-matrix multiplications defining the MPS state), the corresponding lines are joined together. As a result, the graphical representation of an MPS state is made by several elementary three leg tensors (small blue boxes in Fig. 1) connected by a line. In panel (a) of Fig. 1, we illustrate an MPS state for $N = 12$ constituents.

The locality of the interactions allows also to approximate the operator $U(\delta t)$, for $\delta t \ll 1$, at arbitrary order in δt as a matrix product operator (MPO). A MPO is an operator of the form $\hat{O} = \sum_{i_1\cdots i_N, j_1\cdots j_N} o^{i_1\cdots i_N}_{j_1\cdots j_N}\,|i_1, \cdots i_N\rangle\,\langle j_1\cdots j_N|$, and $o^{i_1\cdots i_N}_{j_1\cdots j_N} = tr(B^{i_1}_{j_1}\cdot B^{i_2}_{j_2}\ldots B^{i_{N-1}}_{j_{N-1}}\cdot B^{i_N}_{j_N})$, where each B^i_j is again a matrix. As a result the full B are now tensors with four indices, and can be represented as geometric shapes with four attached lines. In panel (a) of Fig. 1, the B are represented as pale-blue circles, and contracted to represent the operator $U(\delta t)$ for a chain of $N = 12$ constituents.

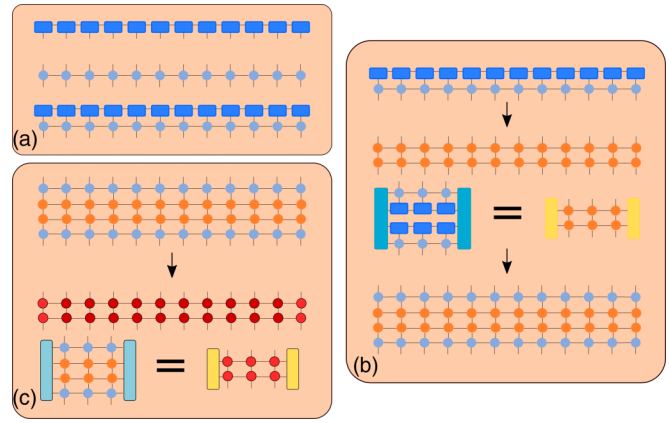

FIG. 1. Tensor network scheme for the proposed algorithm. We use the standard tensor network notation where geometric shapes are tensors and their indices are represented by legs. Tensor contractions are represented by lines joining two different shapes. (a) An initial state that can be represented by a tensor network is evolved for a short time. The initial state is represented as a blue MPS, the evolution is encoded by a pale-blue MPO. The evolved system is represented by the contraction of the MPS and the MPO. (b) The evolved state becomes highly entangled and thus we approximate it with a mixed state represented here by an orange MPDO. The MPDO is obtained variationally by imposing that its reduced density matrices up to distance m coincide exactly with those of the evolved state. Here $m = 3$. Once the best MPDO approximation of the evolved state is obtained, the system is evolved again for short times. (c) The subsequent dynamics increases again the complexity beyond the one we can deal with. We repeat the approximation by using an MPDO with lower operator-Schmidt rank (in red in the figure). During the approximation we always force the local indistinguishability of the approximate state and the evolved one, up to blocks of size m.

The size of the B^i_j matrices increases exponentially as we want to get higher order approximations to $U(\delta t)$. As a result, one typically sticks to relatively low-order approximations of $U(\delta t)$ in δt (e.g., fourth order) and carefully reduces the δt in order to get the required accuracy. We can thus assume that the matrices B^i_j have a fixed rank D_B.

We can perform a single step of time evolution (the TE part of the algorithm) in the tensor network notation by joining the appropriate lines of the MPO and the MPS in order to perform the required matrix vector multiplication. The TE is represented in the lower part of panel a) of Fig. 1, where we compute $|\psi(t_1)\rangle = U(\delta t)\,|\psi(0)\rangle$ for $|\psi(0)\rangle$ expressed as a MPS and $U(\delta t)$ encoded by a MPO.

The graphical representation makes explicit that $|\psi(t_1)\rangle$ is again a MPS, with individual tensors given by $\tilde{A}^j = \sum_i A^i B^j_i$. The bond dimension of $\tilde{A}^j$ has increased from D to DD_B. This fact implies that the process cannot be iterated arbitrarily many times since the size of the matrices would increase exponentially growing to DD^n_B after n iterations.

We thus need to introduce an approximation step, that in the original framework is called the block decimation (BD). The idea introduced by Vidal in Ref. [53], is to simplify $|\psi(t_1)\rangle$ by projecting the MPS matrices $\tilde{A}^j$ onto the subspace spanned just by the most relevant Schmidt vectors. These are the vectors with the largest Schmidt weight.

If the state $|\psi(t_1)\rangle$ is slightly entangled, this projection can be done almost exactly and effectively reduces the size of the MPS matrices $\bar{A}^j$ to $\bar{D} \ll DD_B$. In these specific scenarios, one can thus iterate the procedure successfully several times and perform the evolution of the system for moderately long times.

In a generic out-of-equilibrium scenario, however, the entanglement of a partition of the state grows linearly in time [11]. This means that the number of degrees of freedom required to describe a block of the system grows exponentially in time and the BD truncation step of the standard TEBD algorithm produces a $\bar{D} \simeq DD_B$. The truncation step thus fails to reduce the computational cost of the dynamic and the TEBD evolution remains exponentially expensive.

In generic cases, the TEBD simulations are limited to short times since very soon the required computational resources exceed the available ones. Though we have presented the standard TEBD algorithm the same reasoning applies to any algorithm trying to perform the time-evolution of a state in a MPS form.

Here we present an alternative algorithm, that aims at using a different approximation step to the BD of the TEBD and a different encoding of the state. Similarly to the TEBD algorithm, our algorithm starts with an exact small step of time evolution δt, as illustrated in panel a) of Fig. 1. We also assume that initially the state of the system is encoded in an MPS. We assume that during the short-time evolution generated by the MPO encoding $U(\delta t) = \exp(-iH\delta t)$, the rank of the MPS increases to a value we can still safely encode.

We want to be able to iterate arbitrarily many time the procedure in the cases were we know that the rank of the MPS would increase exponentially with the number of iterations. We thus need to trade the MPS representation for a different one that should make the algorithm scalable to larger times.

We indeed know that (at least for large-enough times) the complexity of the evolved states is encoded in very nonlocal correlations, and the corresponding states are locally indistinguishable from simpler mixed states. This is indeed the essence of thermalization and suggests we should try to use mixed-states rather than pure ones.

In order to find such mixed states, we first compute the reduced density matrix of a region of m spins, by tracing out the remaining $N - m$ spins. This is graphically represented in panel (b) of Fig. 1, where the contractions of all the spins to the left and right of the $m = 3$ region are represented by vertical rectangles. The resulting reduced density matrix of three spins is encoded in the tensor network contraction shown on the left of the second line of panel (b) of Fig. 1.

We proceed by performing a Schmidt decomposition of the reduced density matrix expressing the result as a matrix-product density operator, MPDO [33,57] [shown in orange in the second line of panel (b) of Fig. 1]. Appealing to the translational invariance of the state we neglect the boundary terms in the TN contraction of the reduced density matrix of the state, and use the local MPDO tensor in order to build a trial mixed state. That state is mixed, but not yet locally indistinguishable from the evolved pure state. We thus start the variational optimisation that will ensure the local indistinguishability.

Morally thus, the algorithm consists in trading the evolved state [the first line of the panel (b)] for a mixed state $\rho(0)$ encoded by a MPDO represented in orange in the second line of the panel. The tensors defining the MPDO are variationally optimized, by starting from the tensors obtained from the Schmidt decomposition of the reduced density matrix of a region as we just described.

The cost function of the optimisation (a measure of the distance between the original reduced density matrix and the one obtained from the mixed state) forces the resulting mixed state to become locally indistinguishable from the evolved state. This condition is encoded in the equality in the third line of the panel. There the vertical rectangles (blue on the left and yellow on the right) encode the contraction of the tensor network originating from tracing the constituents outside the region we are interested in and can be easily computed with standard tensor network techniques.

We stress once more that the choice of a local cost function for the variational optimisation of the tensors, together with trading pure states for mixed states, constitute the main differences with respect to the MPS based algorithm. If most of the complexity of the evolved state comes from correlations at large distances (as it does in simple quenches), the MPDO bond dimension (that encodes the correlations at short distances) can be reduced at much smaller value than the bond dimension required to describe the original state.[3]

The maximum MPDO Schmidt rank is also fixed by the available computational resources as in any other tensor network algorithm. In addition to the MPDO Schmidt rank, the size of the region over which the MPDO and the original state are indistinguishable constitutes a new refinement parameter m. When $m \to N$, where N is the system size, we are morally very close to MPS based algorithms. Here we thus focus on the opposite limit, where we expect our algorithm to strongly deviate from the standard ones. We want to characterize the algorithm at fixed $m \ll N$. This is the reason why in Fig. 1 we have presented the case of $m = 3$.

As for the standard TEBD algorithms, once the optimal MPDO is found, we iterate the procedure, as shown in panel (c) of Fig. 1. Here we evolve the system for a certain extra time $\rho(t) = U^\dagger(t)\rho(0)U(t)$, shown in the first line of the panel, and then we truncate its operator Schmidt rank to the pre-established maximal value obtaining the MPDO represented in red in the second line of the panel. The truncation is performed always variationally, without affecting the local correlations as a consequence of the equality in the third raw of the panel.

Summarising, the main idea is to transform the entanglement present in the initial state into mixture, something that is natural in the context of thermalisation at large times. In order to perform this transformation gradually, starting already at relatively short times, we need to force that the mixed states we use are locally indistinguishable from the evolved state.

[3]A simple example is the state of four spin 1/2 constituents $|S(24)S(13)\rangle$, where the $S(ij) = \frac{1}{\sqrt{2}}(|0_i 0_j\rangle + |1_i 1_j\rangle)$. This state written as an MPS $c^{i_1,i_2,i_3,i_4} = Ai_1Ai_2Ai_3Ai_4$ requires A with bond dimension 2. However, the reduced density matrix $\rho(23)$ is the tensor product $\rho(2)\rho(3)$ and thus has operator Schmidt rank 1.

Our algorithm thus implements Jayne's principle [58,59], we are designing an approximate dynamics where at each step the entropy grows due to the fact that some of the generated entanglement is transformed into mixture. At the same time, the "relevant" conserved quantities (i.e., conserved quantities built out of local densities) are protected from the approximations and thus kept constant. We thus expect that, as a consequence of the robustness of the equilibration, the process will equilibrate to a state locally indistinguishable from the DE. Furthermore, in the process we avoid diagonalizing the full Hamiltonian [60], something unavoidable if trying to directly construct the DE.

While trading entanglement with mixture is clearly possible at very long time (this is, in the end, the essence of thermalisation), we need to understand if this is feasible at the early stages of the evolution. We thus need to understand if mixed states that are locally indistinguishable from the states produced in early stages of the evolution exist, how to construct them, and the effects they induce once used at a given time as the starting point for the subsequent evolution.

Since these are general questions that do not depend on the tensor-network formulation of the problem, we address them in the context of free-fermionic models. This allows us to separate any methodological difficulty from the physical effects that such approximation will produce. Such methodological difficulties include for example: the choice of the norm to use in order to force the equalities in Fig. 1 that define the MPDO; assuming that such MPDO exists how to construct an initial guess for it that can be variationally improved; how to design a TN algorithm guaranteed to converge to the optimal MPDO starting from the initial guess; what is the extra effect of the finite operator Schmidt rank.

The relevant states of free-fermionic systems are Gaussian (see Appendix A). As a specific example we will consider the transverse field Ising model

$$H(\theta) = -\sin(\theta)\sum_{i=0}^{N-1}\sigma_i^x\sigma_{i+1}^x - \cos(\theta)\sum_{i=0}^{N-1}\sigma_i^z, \tag{3}$$

that can be re-expressed as a free-fermionic Hamiltonian

$$H(\theta) = -\sin(\theta)\sum_{i=0}^{N-1}[a_i^\dagger a_{i+1} - a_i a_{i+1}^\dagger + a_i^\dagger a_{i+1}^\dagger - a_i a_{i+1}] - \cos(\theta)\sum_{i=0}^{N-1}[a_i^\dagger a_i - a_i a_i^\dagger]. \tag{4}$$

Because of the Wick theorem a generic Gaussian state is fully characterized by the two point correlation functions which can be organized in the so called symbol or correlation matrix [61–63]

$$\Lambda_{i,j} = \langle \vec{\alpha}_i \vec{\alpha}_j^\dagger \rangle, \tag{5}$$

where $\vec{\alpha}^\dagger = (a_1, a_2, \ldots, a_N, a_1^\dagger, a_2^\dagger, \ldots, a_N^\dagger)$ is the collection of annihilation and creations operators for every site.

We benchmark our algorithm by studying the out-of-equilibrium evolution generated by a sudden quench of the Hamiltonian. We start from the ground state of the Hamiltonian (4) for a given θ_0, $H(\theta_0)$ encoded in the correlation matrix Λ_0 and we let it evolve with an Hamiltonian having the same structure, but defined with a different value of θ, $H(\theta)$.

The out-of-equilibrium evolution of free-fermionic systems can be computed exactly providing the ideal setting for benchmarking our approximate algorithm as we explain in detail in Appendixes A and B.

The steps of the algorithm outlined in Fig. 1 can be implemented directly at the level of the correlation matrices. In particular, the truncation step corresponds to defining a truncated matrix $T_m(\Lambda)$, with $m \in [0, \lfloor \frac{N}{2} \rfloor]$, obtained from Λ by setting all the matrix elements corresponding to correlations at distances $d > m$ to zero. For every finite-size system made by N constituents, as m grows to $m = \lfloor \frac{N}{2} \rfloor$, $T_m(\Lambda) = \Lambda$ and thus the approximation becomes exact. $T_m(\Lambda)$ indeed preserves all the reduced density matrices consisting of $m+1$ sites and, as a result, all the expectation values of local operators with support on $m+1$ consecutive sites thus implementing exactly the equality in the panels (b) and (c) of 1.

As an example, in the quenches discussed here, $m \geqslant 1$ is enough to conserve the energy of the system since the total energy for a transverse field Ising Hamiltonian (4) is the sum of operators with support on only two consecutive sites. For a generic Gaussian fermionic Hamiltonian sum of operators with support on at most l neighboring sites, the conservation of the energy is enforced by choosing $m \geqslant (l-1)$.

At last, the truncation maps translation-invariant states to translation-invariant states, thus preserving translation invariance for every choice of m. We can thus build an approximate time evolution algorithm by approximating Λ with $T_m(\Lambda)$ at every step of the evolution. In the specific case of the free fermions, the algorithm presented in Fig. 1 translates in the following pseudocode.

Algorithm 1 Truncated time evolution of precision m

```
procedure Trunc-Evolv (Λ, N_s, δt, m)
    t := 0
    while t < N_s do
        Λ := T_m(Λ)                      ▷ Truncation step
        Λ := Evolve(Λ, H(θ_t), δt)       ▷ Evolution step
        t := t + 1
    end while
    return Λ
end procedure.
```

The evolution time step is performed via exact diagonalisation on the space of the symbol matrices that scales linearly with the dimension of the system. Details on the evolutions are reported in Appendix B.

While the above algorithm could give the illusion that mixed states sharing the same local reduced density matrices with a given state could always be found for Gaussian states, this is not the case. Even though the truncation step preserves the local reduced density matrices of the system it does change the global state. We note, for example, that changing from a finite number to 0 the out-of-diagonal elements of a matrix, in general modifies its eigenvalues. The actual change can only be found by diagonalising the matrix before and after the truncation. As a result, the approximation that we are

performing by zeroing the correlation at distances larger than m can in principle spoil the positivity of the state.

If the above truncation spoils the positivity of the state, this means that we would not be able to find a state in the Hilbert space represented by the correlation matrix we are using. This does not exclude that there could be another mixed state that is still locally indistinguishable from the state we want to approximate, but at least tells us that this state is possibly hard to identify. We will monitor this specific aspect of the algorithm in the numerical analysis.

Before moving to the numerical results we note that the loss of information due to the truncation of the correlations makes the approximate dynamics not unitary. This is somehow expected. We are indeed trying to obtain a good approximation of the Gaussian diagonal ensemble $\rho_{\mathrm{GDE}(H)}$ whose knowledge, in general, is not sufficient to recover the initial state of the quench.

As a word of caution, our exact results refer both to the full out-of-equilibrium dynamics of the system and to the Gaussian state ρ_{GDE} (Gaussian diagonal ensemble [64]) built from the symbol matrix Λ_{DE} (5) of the DE. In general, this state can be different from the actual diagonal ensemble ρ_{DE}, in the specific case we consider here, the two states are locally indistinguishable. With a slight abuse of notation we will thus refer to the ρ_{GDE} as ρ_{DE}.[4]

IV. NUMERICAL RESULTS

We study the dynamics for the quench $\theta : \frac{\pi}{4} + 0.1 \to \frac{\pi}{4} + 0.3$ of the Hamiltonian (4), a quench inside the ordered phase. The results obtained for different quenches both in the disordered phase and across the phase transition are qualitatively similar as can be checked in our Appendix C. We compare different system sizes, $N = 1500$ sites (that we use as the thermodynamic limit) and smaller system sizes. For $N = 1500$, we compute the exact post-quench dynamics for very long times, up to the corresponding recurrence time $T_R \propto 1500$. These are the results we consider exact and we use as a benchmark.

As an intermediate system we consider $N = 200$ sites. For this system, we compute the dynamics for all the admitted values of the parameter m up to the time T_R. In all scenarios, we use time steps of length $\delta t = 0.25$. The smallest system we consider contains $N = 41$ sites since its exact evolution requires similar computational resources to the one required by our approximation of the larger systems.

We indicate with $n = a^\dagger a$ the single site occupation operator (the choice of the specific site is irrelevant since the system is translationally invariant). We represent as $\rho_N(t, m)$ the density matrix of the system of N sites evolved to time t with the truncated algorithm with a value of the refinement parameter m (when m is not explicitly specified we are referring to the state evolved exactly). The expectation value of an operator O on a state ρ is indicated as $\langle O \rangle_\rho = \mathrm{Tr}[\rho O]$.

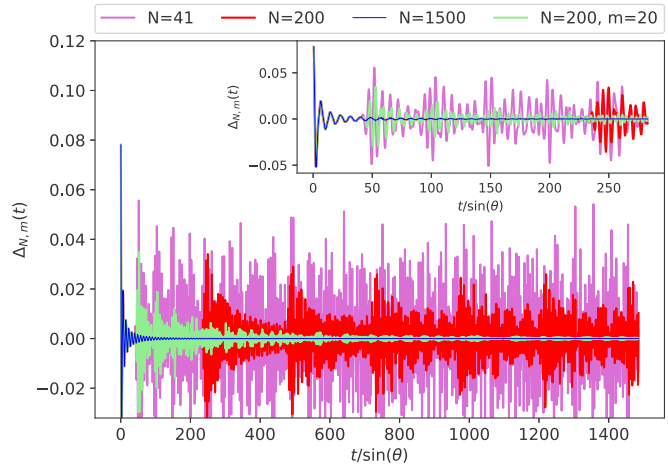

FIG. 2. Time evolution of the quantity $\Delta_{N,m}(t) := \langle n \rangle_{\rho_N(t,m)} - \langle n \rangle_{\mathrm{GDE}}$ for different values of the parameters N and m. In the inset, a zoom on the first part of the dynamics where the recurrence effects for two exacts evolution and the approximation error deriving from the truncations are visible. In the main picture, we plot the evolution for long times. The truncated dynamic converges towards the GDE more slowly than the exact one.

In Fig. 2, we focus on characterising the dynamics of n. All other local operators behave similarly, as we show in Appendix D where we focus on the evolution of the two sites reduced density matrices that encode the expectation value of arbitrary operators defined on two consecutive sites.

We plot the deviation of the dynamics of the single site occupation n from its equilibration value given by the GDE, for several systems evolved both exactly and approximately

$$\Delta_{N,m}(t) := \langle n \rangle_{\rho_N(t,m)} - \langle n \rangle_{\mathrm{GDE}}. \tag{6}$$

The equilibrium value of $\langle n \rangle_{\rho_{1500}(t)}$ tends algebraically towards the value predicted by the GDE. This is a consequence of the general results about the equilibration rate (measured as the damping of the of the envelope of the oscillations in Fig. 2) discussed in [65,66]. The specific operator we are considering converges towards the GDE as a power law, proportional to $(t^{-\frac{3}{2}})$. This rate of convergence is in perfect agreement with the predictions for the thermodynamic limit contained in Refs. [31,67], confirming that the size of the system is large enough to be considered infinite.

In the exact dynamics of the smaller systems ($N = 40$ and 200), we can clearly identify the recurrence effects by the rebirth of large oscillations at later times. It is worth noting that before the recurrence effects become evident, the dynamics of the local observable is the same for all the sizes of the systems we have considered. This is easier to observe in the inset of 2 representing a zoom of the main plot for short times, $\frac{t}{\sin(\theta)} \in [0, 280]$. There we can also appreciate that, as expected, the recurrence time is proportional to the size of the system (in the thermodynamic limit the proportionality constant is the maximum group velocity of the pseudoparticles [11,30–32]).

[4] In general, the possible discrepancies between ρ_{GDE} and ρ_{DE} have already been largely studied in the literature, e.g., ρ_{GDE} has been characterized numerically in Ref. [40] (where it is called *fully constrained thermodynamic ensemble*) and through the recent analytical calculations presented in Refs. [65,66] (where ρ_{GDE} is called *Gaussian generalized Gibbs ensemble*), and we thus refer the interested reader to those publications.

In the plot, we also present the truncated dynamics, $\langle n\rangle_{\rho_{200}(t,20)}$. The choice of $m = 20$ implies that the truncation step always preserves the reduced density matrices of all the sub-systems of $m + 1 = 21$ consecutive sites and for each site it preserves all the correlation with $2m + 1 = 41$ sites. In order to understand the difference between our truncation scheme and the evolution of a small finite system, we also compare the results of the approximate dynamics with those of the exact dynamics for a small system of exactly $N = 41$ sites.

As expected, the truncation does not affect the dynamics at short time. Since the initial state is the ground state of a gapped Hamiltonian its correlation functions decay exponentially with the distance [2,3,7]. During the initial steps of the evolution $\langle n(t)\rangle_{\rho_{200}(t,20)}$ is extremely close to $\langle n(t)\rangle_{\rho_{200}(t)}$. When the correlations spread to distances larger than m, the approximation induced by the truncation becomes evident.

It is instructive to compare $\rho_{41}(t)$ with $\rho_{200}(t, 20)$. In the exact evolution of the small system, the correlated regions spread apart but eventually, due to the periodic boundary conditions, meet again. They meet when each correlation front has traveled through half of the system, in this case 21 sites. When they meet, the recurrence effects they produce disturb the equilibration process of the system.

In contrast, in the truncated evolution the correlations are destroyed once spread further than 21 sites. Erasing such correlations completely changes the dynamics that deviates both from the one of the small periodic system and from that of the larger (practically infinitely large) system.

In order to quantify these modifications, we compute the truncated dynamics far beyond the recurrence time of the system with $N = 2m + 1 = 41$. In the main figure, we observe how $\langle n\rangle_{\rho_{200}(t,20)}$ slowly converges towards a value close to the one predicted by the GDE. We call $e(m)$ the value towards which each truncated evolution with parameter m converges. We need to both characterize how $e(m)$ depends on m and how fast the truncated dynamics converges to $e(m)$.

Both analyses are performed in Fig. 3 where we study the trend of convergence of the truncated dynamics towards its equilibration value $e(m)$. We furthermore study the dependence of the equilibration value $e(m)$ from m.

Considering the time interval during which the approximation induced by the truncated dynamic is manifest we study the evolution of the quantity $\log_{10}|\langle n\rangle_{\rho_N(t,m)} - e(m)|$.

We perform a linear fit on both the exact and truncated dynamics. For the exact dynamics we considered $e(\infty) = \langle n\rangle_{\rm GDE}$ as equilibration value, in this case the slope of the fitting line is $\approx 3/2$ as expected. For the truncated evolution we notice that the rate of convergence towards $e(m)$ is qualitatively similar to the one of the exact dynamics.

At this stage it is important to notice that the exact dynamics of a finite size system will always present recurrences, while the truncated dynamics equilibrates to $e(m)$ for every value of m. The dependence of $e(m)$ on m is addressed in the inset of Fig. 3. The data suggest a dependence

$$e(m) = e^{-m^{\gamma}} + \langle n\rangle_{\rm GDE} \tag{7}$$

with a value of $\gamma = 0.642 \pm 0.003$ extracted by performing a best fit of Eq. (7) to our data.

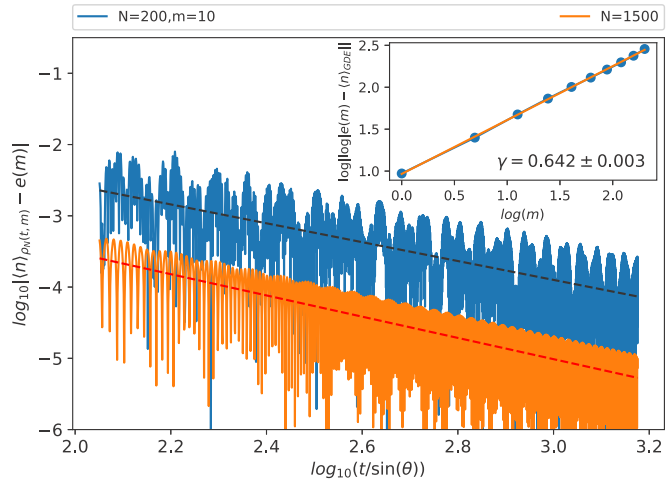

FIG. 3. Logarithmic difference between $\langle n\rangle_{\rho_N(t,m)}$ and the expected equilibration value at a given m, $e(m)$, as a function of the logarithm of time. The exact dynamics converges algebraically to $\langle n\rangle_{\rm GDE}$. The approximate dynamics converges algebraically to $e(10)$. The two dotted lines are linear fits to the data of the dynamics. The quantity $\langle n\rangle_{\rho_N(t)}$ converges to $\langle n\rangle_{\rm GDE}$ as $t^{-\frac{3}{2}}$ for $t < T_R$, where T_R is the recurrence time for the given N. We qualitatively see that the truncated dynamics converges towards $e(10)$ with a similar trend. (Inset) Here we address the dependence of $e(m)$ on m. We plot the log-log difference between the equilibration values $e(m)$ and $\langle n\rangle_{\rm GDE}$ as a function of $\log_{10}(m)$. The linear dependence suggests that $e(m)$ converges towards $\langle n\rangle_{\rm GDE}$ as $(e(m) - \langle n\rangle_{\rm GDE}) \sim e^{-m^{\gamma}}$. Our best fit gives an estimate $\gamma = 0.642 \pm 0.003$.

While we have focused here on a specific local observable and a specific quench protocol, similar results are obtained for all other local observables and quench protocols as shown in Appendixes C and D.

We now turn to characterize the state of the system we obtain after the truncation steps. We first check that, as already mentioned, the purity of $\rho_{200}(t, m)$ decreases during the evolution encoding the fact that the state becomes mixed. The truncation step of the algorithm adds mixedness to the global system, while at the same time (for $m > 1$) conserving local densities, in perfect accordance with Jayne's principle.

In order to confirm this, we consider the reduced state of a block of 100 consecutive sites described by the reduced density matrix $\rho_N^{[100]}(t, m) = Tr_{[101,\ldots,N]}[\rho_N(t, m)]$.

We study the evolution of the second Renyi entropy, defined for generic density matrix ρ as $S_2 = -\log_{10}(\mathrm{Tr}[\rho^2])$ in Fig. 4 where we plot the time evolution of $|S_2(\rho_N^{[100]}(t, m)) - S_2(\rho_{\rm GDE}^{[100]})|$, in logarithmic scale, for different values of the parameters N and m.

For the exact dynamics with $N = 200$, S_2 grows close to the value of $S_2(\rho_{\rm GDE}^{[100]})$ before starting to decrease as a result of the recurrence. It then oscillates, with a frequency fixed by the size of the system.

In the truncated dynamics, correlations are not allowed to return into the partition, therefore, once spread outside, they are lost forever. We see that, indeed, the entropy always increases getting closer to $S_2(\rho_{\rm GDE}^{[100]})$ as m increases.

It is important to check if the states generated by our approximate dynamics are physical. *A priori*, the symbol

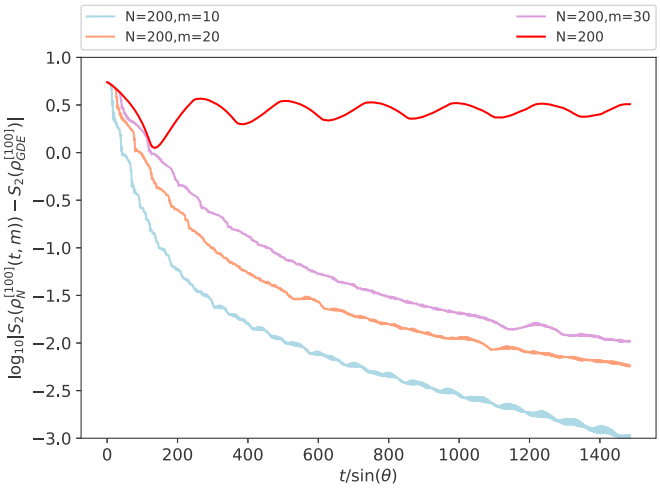

FIG. 4. Time evolution of $|S_2(\rho_N^{[100]}(t,m)) - S_2(\rho_{\mathrm{GDE}}^{[100]})|$ in logarithmic scale for different values of the parameters N and m. In the exact dynamics, the recurrence effects are evident from the oscillatory behavior of the dynamics. In the truncated dynamics, correlations are not allowed to return into the partition, therefore, once spread outside, they are lost forever. We see that indeed the entropy always increases getting closer to $S_2(\rho_{\mathrm{GDE}}^{[100]})$ as m increases.

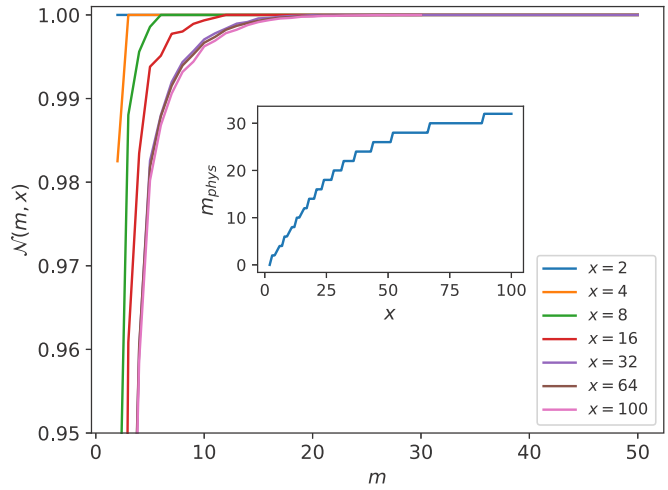

FIG. 5. The value of $\mathcal{N}(m,x)$ versus m is plotted for different dimensions x of the reduced matrix $\overline{\rho}(m)_x$. When $\mathcal{N}(m,x)=1$ then $\overline{\rho}(m)_x$ is physical. (Inset) Minimum value of the precision m_{phys} for a specific x such that $\overline{\rho}(m)_x$ is physical. It is remarkable that already for moderate values of m the approximate state is physical over a large range of distances.

matrix obtained after the truncation step is not guaranteed to represent a legitimate state of the free-fermionic Hilbert space. A matrix is a density matrix only if it is positive semidefinite. Checking if a matrix is positive requires diagonalising it, and, since the size of the matrix increases exponentially with the size of the system, this becomes unfeasible already for very small systems. In the case of tensor networks, the task is shown to be NP-hard in the dimension of the system [68]. Conversely, the symbol matrix Λ of a free-fermionic system represents a physical state if its eigenvalues are in the interval [0,1] [62].

In order to check if on average the physicality is conserved, we consider the density matrix $\bar{\rho}(m)$ associated to the time average of the symbol matrices for each m,

$$\overline{\Lambda}(m) = \frac{1}{N_s}\sum_{t=1}^{N_s}\Lambda(t\cdot\delta t, m), \tag{8}$$

where N_s is the number of steps considered for the evolution. This check requires diagonalising the symbol matrix, an operation that scales polynomially with the system size. The eigenvalues of Λ appear in couples $(\lambda_i, 1-\lambda_i)$. Λ is nonphysical if it contains at least one eigenvalue smaller than 0 (hence its partner will be larger than 1).

We thus define the quantity $\mathcal{N}(m,x)$ that is 1 minus the sum of the negative eigenvalues of $\Lambda(m)_x$,

$$\mathcal{N}(x,m) = 1 - \frac{||\Lambda(m)_x||_{l=1}-1}{2} = 1 - \sum_i \frac{|\lambda_i|-\lambda_i}{2}, \tag{9}$$

where $\Lambda(m)_x$ is the symbol matrix of $Tr_{[1,\ldots,N-x]}[\overline{\rho}(m)] = \overline{\rho}(m)_x$ and $\{\lambda_i\}_i$ are the eigenvalues of $\Lambda(m)_x$.

$\mathcal{N}(m,x)=1$ for a physical $\overline{\rho}(m)_x$, since as mentioned all the eigenvalue are in this case positive in the interval between 0 and 1. $\mathcal{N}(m,x)$ decreases as the absolute value of the sum of negative eigenvalues of $\Lambda(m)_x$ increases.

In Fig. 5, we plot $\mathcal{N}(m,x)$ versus m for different values of x. We can see that for large enough m the reduced density matrices of $\overline{\rho}(m)$ become physical for every chosen size x. In the inset, we plot the minimum value of precision m_{phys} required for $\overline{\rho}(m)_x$ to be physical for every choice of its size x.

This fact should be related to the finite correlation length present in the GDE. In order to describe correctly the expectation value of a local operator, we just need to embed the local system into a larger system whose size exceeds the correlation length of the desired state (see, e.g., Refs. [69–73]).

V. CONCLUSION

We have identified some robust aspects of the out-of-equilibrium dynamics encoded in the late-time expectation value of local operators after the quench. By exploiting this robustness we have designed an approximate algorithm that allows to predict the relaxed values of local operators with limited computational resources.

The key idea underlying the design of our algorithm is to protect from the approximations the relevant conserved quantities. These are defined as the conserved quantities built out of local densities. The degree of locality of such conserved quantities naturally acts as the refinement parameter of the algorithm allowing to increase the precision of the results by increasing the computational cost.

We have benchmarked the algorithm in the case of free-fermionic systems where the algorithm can be implemented very easily at the level of the correlation matrices. Here the approximation required by the algorithm corresponds to discarding those elements of the correlation matrices (5) that are at distance larger than a certain cutoff distance m from the diagonals.

We have observed that for modest values of m the results are in good agreement with the exact ones. Furthermore,

their precision improves exponentially as we increase the computational resources.

The next step is to check if the same picture holds in the presence of strong interactions both in the integrable and nonintegrable scenarios, by implementing the generic version of the algorithm using tensor networks along the lines of the scheme presented in Fig. 1. It would also be interesting to compare and relate this approach with the existing complementary one proposed in Refs. [17,26,74–78].

ACKNOWLEDGMENTS

We acknowledge the discussion on the topic with Frank Verstraete, Marie Carmen Banuls, and Frank Pollman. J.S. was supported by the doctoral training partnership of EPSRC (DTP 2016-2017) Studentship N.1812047 at the University of Strathclyde. L.T. was supported by Ramon y Cajal program of the MICINN of the Spanish Government. While this paper was under review several proposals have appeared that design and benchmark alternative algorithms for simulating the long-time dynamics of the many-body systems efficiently [79–81].

APPENDIX A: FERMIONIC GAUSSIAN SYSTEMS

The generic quadratic (or Gaussian) fermionic Hamiltonian on N sites can be written as

$$H = \frac{1}{2}\sum_{i,j=1}^{N-1}[A_{i,j}a_i^\dagger a_j - \overline{A}_{i,j}a_i a_j^\dagger + B_{i,j}a_i a_j - \overline{B}_{i,j}a_i^\dagger a_j^\dagger], \quad \text{(A1)}$$

where $A_{i,j}, B_{i,j} \in \mathbb{C}$, $A = A^\dagger$, $B^T = -B$ and the annihilation and creation operators a_i and $a_i^\dagger$ obey the anticommutation relations $\{a_i^\dagger, a_j\} = \delta_{i,j}$, $\{a_i^\dagger, a_j^\dagger\} = \{a_i, a_j\} = 0$.

In the main text, we restricted to the single parameter Hamiltonian $H(\theta)$ (4) defined by the matrices

$$\begin{aligned} A(\theta)_{i,j} &= -f_{N,i,j}\sin(\theta)(\delta_{i+1,j} + \delta_{i,j+1}) - 2\cos(\theta)\delta_{i,i}, \\ B(\theta)_{i,j} &= f_{N,i,j}\sin(\theta)(\delta_{i+1,j} - \delta_{i,j+1}), \end{aligned} \quad \text{(A2)}$$

with the term

$$f_{N,i,j} = \begin{cases} -(-1)^{\langle N\rangle}, & \text{if } i \vee j = N \\ 1, & \text{otherwise} \end{cases} \quad \text{(A3)}$$

necessary for the antisymmetrisation with periodic boundary condition.

This one parameter Hamiltonian is the mapping to fermions of the 1D transverse field Ising model on N sites and periodic boundary condition

$$H(\theta) = -\sin(\theta)\sum_{i=0}^{N-1}\sigma_i^x\sigma_{i+1}^x - \cos(\theta)\sum_{i=0}^{N-1}\sigma_i^z, \quad \text{(A4)}$$

where $(\sigma_i^x, \sigma_i^x, \sigma_i^z)$ are the Pauli matrices on site i, $\theta \in [0, \frac{\pi}{2}]$ and N is the number of sites [82].

A fermionic Gaussian state is a ground or thermal state of a quadratic fermionic Hamiltonian. Using Wick's theorem it is possible to show that Gaussian states are completely characterized by the collection of their two-point correlators

$$\Lambda_{i,j}^{TL} = \mathrm{Tr}[\rho a_i^\dagger a_j], \quad \text{(A5)}$$

$$\Lambda_{i,j}^{TR} = \mathrm{Tr}[\rho a_i^\dagger a_j^\dagger], \quad \text{(A6)}$$

where the correlators $\mathrm{Tr}[\rho a_i^\dagger a_j]$ and $\mathrm{Tr}[\rho a_i^\dagger a_j^\dagger]$ are said to be a correlators at distance $d_{i,j}$, where $d_{i,j} \equiv \min(|i-j|, |N-(i-j)|)$. We have that Λ^{TL} is Hermitian and Λ^{TR} is skew-symmetric. The two-point correlators can be arranged in the block matrix

$$\Lambda = \left[\begin{array}{cc} \Lambda^{TL} & \Lambda^{TR} \\ -\Lambda^{TR*} & \mathbb{I} - \Lambda^{TL T} \end{array}\right],$$

called the symbol matrix [61]. The symbol matrix is Hermitian and for any admissible symbol matrix of a physical fermionic system, the eigenvalues have to be in the interval [0,1].

The two-point correlators of translational invariant states depend only on the distance, thus the elements $\Lambda_{i,j}^{TL}$ simplify to elements of the circulant matrices $\Lambda_{d_{i,j}}^{TL}$ which depend only on the distance between the indices.

The space of Gaussian states is closed under evolution induced by quadratic Hamiltonians, thus, if we start with a Gaussian state and evolve it with a Hamiltonian of the form (A1) the knowledge of Λ at any time would completely characterize the state of the system.

The reduced state over a set of sites S is still a Gaussian state and it is characterized by the symbol matrix of all the two-point correlators with support on S.

APPENDIX B: GAUSSIAN EVOLUTION OF FERMIONIC GAUSSIAN STATES

A generic Gaussian fermionic Hamiltonian H of the form (A1) can always be brought in the form

$$H = \frac{1}{2}\sum_{k=0}^{N-1}\epsilon_k(b_k^\dagger b_k - b_k b_k^\dagger) \quad \text{(B1)}$$

for a specific set of fermionic annihilation and creation operators $b_k, b_k^\dagger$.

The time evolution of the operators $b_k, b_k^\dagger$ with the Hamiltonian H is easily computed as

$$\begin{aligned} b_k(t) &= e^{-i\epsilon_k t}b_i, \\ b_k^\dagger(t) &= e^{i\epsilon_k t}b_k^\dagger. \end{aligned} \quad \text{(B2)}$$

Given a symbol matrix Λ expressed on the basis of the fermionic annihilation and creation operators $a_i, a_i^\dagger$, there exist unitary operation that allows one to express Λ on the basis of $b_k, b_k^\dagger$. In term of these operators, the submatrices of Λ can be written as

$$\begin{aligned} \Lambda_{k,l}^{TL} &= \mathrm{Tr}[\rho b_k^\dagger b_l], \\ \Lambda_{k,l}^{TR} &= \mathrm{Tr}[\rho b_k^\dagger b_l^\dagger]. \end{aligned} \quad \text{(B3)}$$

Using this representation, one is able to compute the time evolution of the correlation matrix elements as

$$\begin{aligned} \Lambda_{k,l}^{TL}(t) &= e^{i(\epsilon_k - \epsilon_l)}\Lambda_{k,l}^{TL}, \\ \Lambda_{k,l}^{TR}(t) &= e^{i(\epsilon_k + \epsilon_l)}\Lambda_{k,l}^{TR}. \end{aligned} \quad \text{(B4)}$$

One can then return to the basis of the annihilation and creation operators $a_i, a_i^\dagger$.

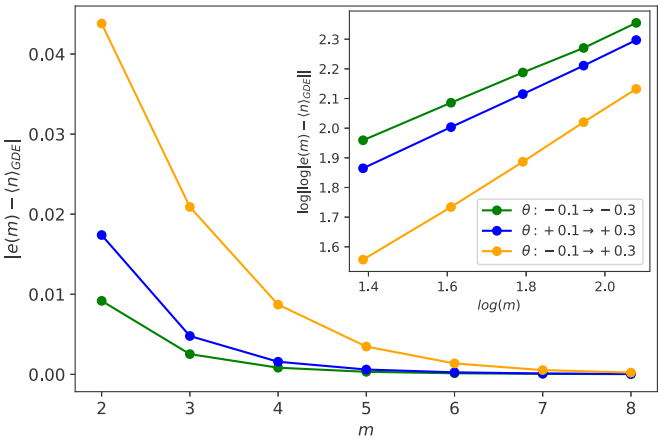

FIG. 6. The difference $|e(m) - \langle n \rangle_{\mathrm{GDE}}|$, where $e(m)$ is the equilibrium value of the local observable n for the truncated evolution of parameter m in the corresponding quench (different quenches correspond to different colors) and $\langle n \rangle_{\mathrm{GDE}}$ is the value of n computed on the corresponding GDE. (Inset) We plot the same data of the main figure, with a suitable scale, in order to check the validity of the ansatz (7).

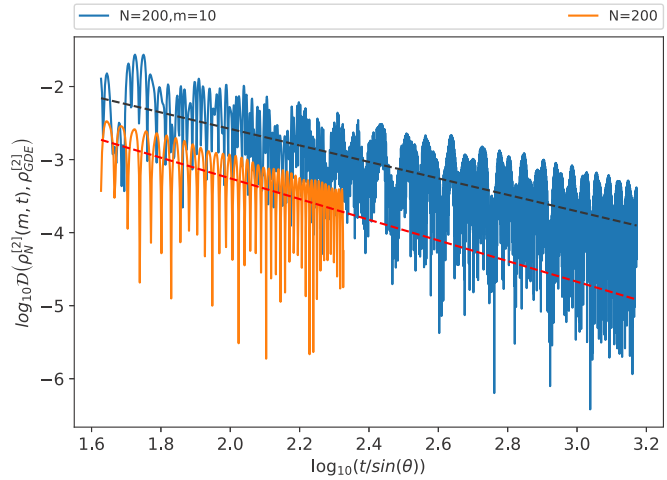

FIG. 7. Time evolution of the logarithm of the trace distance $\mathcal{D}(\rho_N^{[2]}(m,t), \rho_{\mathrm{GDE}}^{[2]})$. Both the exact dynamics as the truncated dynamics locally converge towards the GDE.

APPENDIX C: NUMERICAL RESULTS FOR DIFFERENT QUENCHES

We checked the algorithm for different quenches of the Hamiltonian (4). In the main text, we analysed the dynamic for a quench above the critical point ($\theta = \frac{\pi}{4}$). We study the dynamics for quenches below the critical point ($\theta : \frac{\pi}{4} - 0.1 \to \frac{\pi}{4} - 0.3$) and across the critical point ($\theta : \frac{\pi}{4} - 0.1 \to \frac{\pi}{4} + 0.3$). In Fig. 6, we plot the difference $|e(m) - \langle n \rangle_{\mathrm{GDE}}|$, where $e(m)$ is the equilibrium value of the local observable n for the truncated evolution of parameter m in the corresponding quench (different quenches correspond to different colors). The linear trend in the inset confirms the validity of the ansatz (7).

APPENDIX D: OBSERVABLES INDEPENDENT LOCAL CONVERGENCE

We checked the local convergence of the two-site reduced density matrices $\rho_N^{[2]}(m,t) := Tr_{[3,\ldots,N]}[\rho_N(m,t)]$ towards the two-site reduced density matrix of the GDE $\rho_{\mathrm{GDE}}^{[2]} := Tr_{[3,\ldots,N]}[\rho_{\mathrm{GDE}}]$.

In Fig. 7, we plot the time evolution of the logarithm of the trace distance

$$\mathcal{D}\left(\rho_N^{[2]}(m,t), \rho_{\mathrm{GDE}}^{[2]}\right) = \tfrac{1}{2} Tr\left[\left|\rho_N^{[2]}(m,t) - \rho_{\mathrm{GDE}}^{[2]}\right|\right]. \quad \text{(D1)}$$

The trace distance is a measure of the maximum probability of distinguishing between two states with an optimal measurement.

The two dotted lines are the linear fits for the two distances. The 2×2 reduced system, both for the exact as for the truncated dynamics, converge towards the 2×2 reduced system of the GDE with a similar trend as the one observed in the observable dependent scenario of Fig. 3.

[1] G. Parisi, *Statistical Field Theory* (Addison-Wesley, 1988).
[2] M. B. Hastings, J. Stat. Mech.: Theory Exp. (2007) P08024.
[3] M. M. Wolf, F. Verstraete, M. B. Hastings, and J. I. Cirac, Phys. Rev. Lett. **100**, 070502 (2008).
[4] J. Eisert, M. Cramer, and M. B. Plenio, Rev. Mod. Phys. **82**, 277 (2010).
[5] G. Vidal, Phys. Rev. Lett. **91**, 147902 (2003).
[6] U. Schollwöck, Ann. Phys. (NY) **326**, 96 (2011).
[7] J. Eisert, Model. Simul. **3**, 39 (2013).
[8] S. R. White, Phys. Rev. B **48**, 10345 (1993).
[9] S. R. White, Phys. Rev. Lett. **69**, 2863 (1992).
[10] R. Orús, Annal. Phys. **349**, 117 (2014).
[11] P. Calabrese and J. Cardy, J. Stat. Mech.: Theory Exp. (2005) P04010.
[12] G. De Chiara, S. Montangero, P. Calabrese, and R. Fazio, J. Stat. Mech.: Theory Exp. (2006) P03001.
[13] A. M. Läuchli and C. Kollath, J. Stat. Mech.: Theory Exp. (2008) P05018.
[14] H. Kim and D. A. Huse, Phys. Rev. Lett. **111**, 127205 (2013).
[15] M. Fagotti and M. Collura, arXiv:1507.02678.
[16] M. Kormos, M. Collura, G. Takács, and P. Calabrese, Nat. Phys. **13**, 246 (2017).
[17] C. W. von Keyserlingk, T. Rakovszky, F. Pollmann, and S. L. Sondhi, Phys. Rev. X **8**, 021013 (2018).
[18] M. Collura, M. Kormos, and G. Takacs, Phys. Rev. A **98**, 053610 (2018).
[19] S. Trotzky, Y.-A. Chen, A. Flesch, I. P. McCulloch, U. Schollwöck, J. Eisert, and I. Bloch, Nat. Phys. **8**, 325 (2012).

[20] P. Corboz and G. Vidal, Phys. Rev. B **80**, 165129 (2009).
[21] G. Evenbly and G. Vidal, New J. Phys. **12**, 025007 (2010).
[22] G. Evenbly and G. Vidal, Phys. Rev. B **81**, 235102 (2010).
[23] M. T. Fishman and S. R. White, Phys. Rev. B **92**, 075132 (2015).
[24] G. Evenbly and S. R. White, Phys. Rev. Lett. **116**, 140403 (2016).
[25] J. Haegeman, B. Swingle, M. Walter, J. Cotler, G. Evenbly, and V. B. Scholz, Phys. Rev. X **8**, 011003 (2018).
[26] C. D. White, M. Zaletel, R. S. K. Mong, and G. Refael, Phys. Rev. B **97**, 035127 (2018).
[27] J. Hauschild, E. Leviatan, J. H. Bardarson, E. Altman, M. P. Zaletel, and F. Pollmann, Phys. Rev. B **98**, 235163 (2018).
[28] A. Polkovnikov, K. Sengupta, A. Silva, and M. Vengalattore, Rev. Mod. Phys. **83**, 863 (2011).
[29] V. Alba, Proc. Natl. Acad. Sci. USA **114**, 7947 (2017).
[30] P. Calabrese, F. H. L. Essler, and M. Fagotti, Phys. Rev. Lett. **106**, 227203 (2011).
[31] P. Calabrese, F. H. Essler, and M. Fagotti, J. Stat. Mech.: Theory Exp. (2012) P07022.
[32] P. Calabrese, F. H. L. Essler, and M. Fagotti, J. Stat. Mech.: Theory Exp. (2012) P07016.
[33] F. Verstraete, J. J. García-Ripoll, and J. I. Cirac, Phys. Rev. Lett. **93**, 207204 (2004).
[34] J. M. Deutsch, Phys. Rev. A **43**, 2046 (1991).
[35] M. Srednicki, Phys. Rev. E **50**, 888 (1994).
[36] M. Rigol, V. Dunjko, and M. Olshanii, Nature (London) **452**, 854 (2008).
[37] M. Rigol and M. Srednicki, Phys. Rev. Lett. **108**, 110601 (2012).
[38] L. D'Alessio, Y. Kafri, A. Polkovnikov, and M. Rigol, Adv. Phys. **65**, 239 (2016).
[39] M. Rigol, Phys. Rev. Lett. **112**, 170601 (2014).
[40] M. Rigol, V. Dunjko, V. Yurovsky, and M. Olshanii, Phys. Rev. Lett. **98**, 050405 (2007).
[41] M. Cramer, C. M. Dawson, J. Eisert, and T. J. Osborne, Phys. Rev. Lett. **100**, 030602 (2008).
[42] T. Barthel and U. Schollwöck, Phys. Rev. Lett. **100**, 100601 (2008).
[43] M. Cramer and J. Eisert, New J. Phys. **12**, 55020 (2010).
[44] M. Fagotti and F. H. L. Essler, Phys. Rev. B **87**, 245107 (2013).
[45] T. Langen, S. Erne, R. Geiger, B. Rauer, T. Schweigler, M. Kuhnert, W. Rohringer, I. E. Mazets, T. Gasenzer, and J. Schmiedmayer, Science **348**, 207 (2015).
[46] E. Ilievski, J. De Nardis, B. Wouters, J.-S. Caux, F. H. L. Essler, and T. Prosen, Phys. Rev. Lett. **115**, 157201 (2015).
[47] L. Vidmar and M. Rigol, J. Stat. Mech.: Theory Exp. (2016) 064007.
[48] F. H. Essler, G. Mussardo, and M. Panfil, J. Stat. Mech.: Theory Exp. (2017) 013103.
[49] B. Pozsgay, J. Stat. Mech.: Theory Exp. (2014) P09026.
[50] V. Alba, Phys. Rev. B **91**, 155123 (2015).
[51] M. Kollar and M. Eckstein, Phys. Rev. A **78**, 013626 (2008).
[52] D. M. Gangardt and M. Pustilnik, Phys. Rev. A **77**, 041604(R) (2008).
[53] G. Vidal, Phys. Rev. Lett. **93**, 040502 (2004).
[54] S. R. White and A. E. Feiguin, Phys. Rev. Lett. **93**, 076401 (2004).
[55] S. Paeckel, T. Köhler, A. Swoboda, S. R. Manmana, U. Schollwöck, and C. Hubig, arXiv:1901.05824.
[56] T. Koffel, M. Lewenstein, and L. Tagliacozzo, Phys. Rev. Lett. **109**, 267203 (2012).
[57] M. Zwolak and G. Vidal, Phys. Rev. Lett. **93**, 207205 (2004).
[58] E. T. Jaynes, Phys. Rev. **108**, 171 (1957).
[59] E. T. Jaynes, Phys. Rev. **106**, 620 (1957).
[60] M. Perarnau-Llobet, A. Riera, R. Gallego, H. Wilming, and J. Eisert, New J. Phys. **18**, 123035 (2016).
[61] E. Greplová, Master Thesis, Technische Universität München Max-Planck-Institut für Quantenoptik, Germany (2013).
[62] C. V. Kraus, PhD. Thesis, Technische Universität München Max-Planck-Institut für Quantenoptik, Germany.
[63] T. D. Schultz, D. C. Mattis, and E. H. Lieb, Rev. Mod. Phys. **36**, 856 (1964).
[64] J. Surace (unpublished).
[65] C. Murthy and M. Srednicki, arXiv:1809.03681.
[66] M. Gluza, J. Eisert, and T. Farrelly, arXiv:1809.08268.
[67] L. Bucciantini, M. Kormos, and P. Calabrese, J. Phys. A **47**, 175002 (2014).
[68] M. Kliesch, C. Gogolin, M. J. Kastoryano, A. Riera, and J. Eisert, Phys. Rev. X **4**, 031019 (2014).
[69] S. Hernández-Santana, A. Riera, K. V. Hovhannisyan, M. Perarnau-Llobet, L. Tagliacozzo, and A. Acín, New J. Phys. **17**, 085007 (2015).
[70] M. Kliesch, D. Gross, and J. Eisert, Phys. Rev. Lett. **113**, 160503 (2014).
[71] A. De Pasquale, D. Rossini, R. Fazio, and V. Giovannetti, Nat. Commun. **7**, 12782 (2016).
[72] A. García-Saez, A. Ferraro, and A. Acín, Phys. Rev. A **79**, 052340 (2009).
[73] A. Ferraro, A. García-Saez, and A. Acín, Europhys. Lett. **98**, 10009 (2012).
[74] E. Leviatan, F. Pollmann, J. H. Bardarson, D. A. Huse, and E. Altman, arXiv:1702.08894.
[75] J. Wurtz and A. Polkovnikov, arXiv:1808.08977.
[76] J.-S. Caux and F. H. L. Essler, Phys. Rev. Lett. **110**, 257203 (2013).
[77] J. D. Nardis, L. Piroli, and J.-S. Caux, J. Phys. A **48**, 43FT01 (2015).
[78] J. S. Caux, J. Stat. Mech.: Theory Exp. (2016) 64006.
[79] M. M. Rams and M. Zwolak, arXiv:1904.12793.
[80] C. Krumnow, J. Eisert, and O. Legeza, arXiv:1904.11999.
[81] L. Cao, V. Bolsinger, S. I. Mistakidis, G. M. Koutentakis, S. Krönke, J. M. Schurer, and P. Schmelcher, J. Chem. Phys. **147**, 044106 (2017).
[82] A. Dutta, U. Divakaran, S. Diptiman, B. K. Chakrabarti, T. F. Rosenbaum, and G. Aeppli, (2012).
[83] A. Nahum, J. Ruhman, S. Vijay, and J. Haah, Phys. Rev. X **7**, 031016 (2017).
[84] L. Cevolani, J. Despres, G. Carleo, L. Tagliacozzo, and L. Sanchez-Palencia, Phys. Rev. B **98**, 024302 (2018).